Delamination Specimens for Orthotropic Materials

Zhigang Suo[1]
Division of Applied Sciences,
Harvard University,
Cambridge, MA 02138

A semi-infinite crack in an infinite strip of orthotropic material is analyzed. Analytic expressions for mixed-mode stress intensity factors are derived with only parameter undetermined, which is then extracted from numerical solutions to integral equations. The results are relatively simple and complete, and provide the flexibility to simulate a wide range of practical problems, such as fracture specimens and edge delamination phenomena of woods and fiber-reinforced composites. As an illustration, specimens with transverse splitting from notches are analyzed based on the general solution. The validity of using solutions for an isotropic material to calibrate some testing geometries of orthotropic materials is discussed.

1 Introduction

Cracks in homogeneous, isotropic brittle materials tend to grow under mode I conditions. By contrast, cracks are often trapped, with *mixed-mode* local field, to geometrically particular paths such as the fiber direction of woods and uniaxial fiber reinforced composites, the interface of bimaterial systems, and the adhesive layer between bonded substrates owing to anisotropy and/or inhomogeneity in stiffness and toughness. The mixed-mode fracture problem is not only of fundamental interest, but also of significant technical importance. High apparent toughness under tension in the fiber direction for woods and composites, for example, is largely attributed to crack splitting, or fiber/matrix debonding (Ashby et al., 1985; Marshall and Evans, 1985; Budiansky et al., 1986). Experimental investigations on fracture in woods and composites appear to be initiated by Wu (1967). Recent efforts in this direction are found in Ashby et al. (1985), Marshall and Evans (1985), Prewo (1986), Michalske and Hellmann (1988), and Sbaizero et al. (1988). Research on analogous situations such as adhesive joints and bimaterial interfaces, where mixed-mode fracture is crucial, are found in Liechti and Hanson (1988), Chai (1988), Argon et al. (1989), and Wang and Suo (1990). The present work is motivated in part by the intention of using a four-point bend specimen to conduct fracture tests on fiber-reinforced composites (Sbaizero et al., 1988).

The basic problem analyzed is introduced in Fig. 1(*a*). A semi-infinite crack in an infinite strip of orthotropic material is considered. More specifically, the strip surfaces are traction-free and in the direction of a principal axis of the material. The crack is parallel to these free surfaces, and driven by the edge loads P_i and M_i, the resultant forces and moments per unit width, respectively. The material is taken to be homogeneous and linearly elastic. Both plane-stress and plane-strain deformations will be considered. The analysis provides the complete solutions for the mixed-mode stress intensity factors. The body of paper will be devoted to the representation and application of the major results. Mathematical details are grouped into three appendices, which may be of some interest in themselves.

2 Representation of Stress Intensity Factors

For generally anisotropic materials, Hooke's law can be written as

$$\epsilon_i = \sum_{j=1}^{6} s_{ij}\sigma_j, \quad i = 1, 2, 3, 4, 5, 6. \tag{1}$$

The standard correspondence is adopted, i.e., $\{\epsilon_i\} = \{\epsilon_x, \epsilon_y, \epsilon_z, \gamma_{yz}, \gamma_{zx}, \gamma_{xy}\}^T$, $\{\sigma_i\} = \{\sigma_x, \sigma_y, \sigma_z, \tau_{yz}, \tau_{zx}, \tau_{xy}\}^T$, and $[s_{ij}]$ is a six-by-six symmetric matrix, referred to as the compliance matrix, with 21 independent elements. When the material has an elastic symmetry plane normal to z-axis, the stress-strain relation for the deformation in the (x, y) plane can be reduced to (see Lekhnitskii, 1963)

$$\epsilon_i = \sum_{j=1,2,6} b_{ij}\sigma_j, \quad i = 1, 2, 6 \tag{2}$$

where

$$b_{ij} = \begin{cases} s_{ij}, & \text{for plane stress} \\ s_{ij} - s_{i3}s_{j3}/s_{33}, & \text{for plane strain} \end{cases} \qquad i, j = 1, 2, 6. \tag{3}$$

On the other hand, if the material is orthotropic with x and y-axes coincident with the principal axes of the material, there are only *four* independent elastic constants b_{11}, $b_{12} = b_{21}$, b_{22}, and b_{66}, but $b_{16} = b_{26} = 0$.

For any simply connected domain of orthotropic medium with traction prescribed on its boundary, the stresses should only depend on *two* (rather than three) nondimensional elastic parameters (see Appendix A)

---

[1]Current address: Department of Mechanical Engineering, University of California, Santa Barbara, CA 93106.

Contributed by the Applied Mechanics Division of THE AMERICAN SOCIETY OF MECHANICAL ENGINEERS for publication in the JOURNAL OF APPLIED MECHANICS.

Discussion on this paper should be addressed to the Technical Editor, Prof. Leon M. Keer, The Technological Institute, Northwestern University, Evanston, IL 60208, and will be accepted until two months after final publication of the paper itself in the JOURNAL OF APPLIED MECHANICS. Manuscript received by the ASME Applied Mechanics Division, Nov. 21, 1988; final revision, July 28, 1989.

Table 1 Values and λ and ρ for some materials

Material	$1/\lambda$	ρ
Al (FCC)	1	0.74
Cu (FCC)	1	0.03
Fe (BCC)	1	0.20
Pb (FCC)	1	0.33
Ash	10.5	1.67
Balsa	21.0	2.13
Oak	2.7	1.16
Pine	14.8	1.10
Graphite/Epoxy	9.5	3.34
GY70/Epoxy	42.0	3.36
Boron/Epoxy	14.3	4.91
Graphite/Al	5.0	1.12

$$\lambda=\frac{b_{11}}{b_{22}},\ \rho=\frac{2b_{12}+b_{66}}{2\sqrt{b_{11}b_{22}}}. \tag{4}$$

These parameters measure the anisotropy in the sense that $\lambda=1$ as the material symmetry degenerates to be transversely cubic and $\lambda=\rho=1$ as the material becomes transversely isotropic. The positive definiteness of the strain energy density requires that $\lambda>0$ and $\rho>-1$. Many nondimensional parameters for orthotropic materials other than those in equation (4) have been used in the literature, but none of them have offered the unique feature discussed in Appendix A. In Table 1, the plane-stress values of λ and ρ are listed for some single crystals, woods, and composites (no dramatic differences have been found for the corresponding plane-strain values). It appears from this list that ρ is typically somewhere in the range from 0 to 5, while λ can be significantly greater or less than 1.

The elastic stress field at the crack tip for generally anisotropic body has a square root singularity. Accordingly, stress intensity factors, K_I and K_{II}, can be defined such that the stress at a distance r ahead of the crack tip are given asymptotically by

$$\sigma_{yy}=\frac{K_I}{\sqrt{2\pi r}},\ \tau_{xy}=\frac{K_{II}}{\sqrt{2\pi r}}. \tag{5}$$

For a crack in an orthotropic body, lying in a principal plane and with its front in a principal direction, the relative crack face displacements at a distance r behind the crack tip are

$$\delta_y=8b_{11}\lambda^{-3/4}n\,K_I\sqrt{\frac{r}{2\pi}},\ \delta_x=8b_{11}\lambda^{-1/4}n\,K_{II}\sqrt{\frac{r}{2\pi}}, \tag{6}$$

where the frequently encountered constant n is defined by

$$n=\sqrt{\frac{1+\rho}{2}}. \tag{7}$$

The energy release rate, derived from equations (5) and (6), is related to the stress intensity factors by

$$G=b_{11}n(\lambda^{-3/4}K_I^2+\lambda^{-1/4}K_{II}^2). \tag{8}$$

These results are contained in the work by Sih, Paris, and Irwin (1965). The present normalization is related to theirs by $K_I=\sqrt{\pi}k_1$, $K_{II}=\sqrt{\pi}k_2$. Rearrangements have been made using the two anisotropy measures identified previously to suit our purpose.

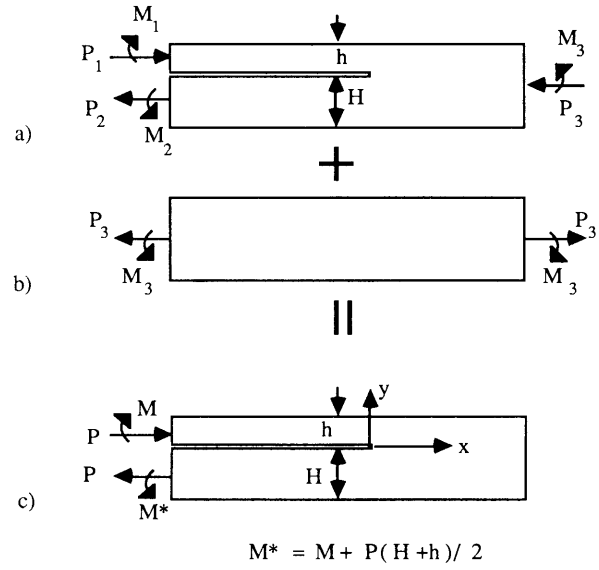

Fig. 1 Conventions and the superposition scheme

The analysis of the problem in Fig. 1(*a*) is now taken up. The aim is to solve for K_I and K_{II} as functions of the loads P's and M's, geometry specifications h and H, and anisotropy measures λ and ρ. Overall equilibrium provides two constraints among the six loads P_i and M_i. Therefore, only four of them are independent, say P_1, P_3, M_1, and M_3. Superposition of the systems in Fig. 1(*a*) and 1(*b*) gives that in Fig. 1(*c*), with P and M given by

$$P=P_1-C_1P_3-C_2M_3/h$$
$$M=M_1-C_3M_3 \tag{9}$$
$$C_1=\frac{1}{1/\eta+1},\ C_2=\frac{6/\eta}{(1/\eta+1)^3},\ C_3=\frac{1}{(1/\eta+1)^3},\ \eta=\frac{h}{H}.$$

Since no stress singularity is present in the beam in Fig. 1(*b*), the stress intensity factors must be identical for both systems in Figs. 1(*a*) and 1(*c*). We will concentrate on the reduced problem in Fig. 1(*c*). Once the latter problem is solved, the solution to the general problem in Fig. 1(*a*) can be constructed by the above relations.

The energy release rate for the system in Fig. 1(*c*) can be computed exactly by using the energy stored in the structure per unit width per unit length far behind the crack tip (e.g., Rice, 1968). The result is a positive definite quadratic in P and M which can be written as

$$G=\frac{b_{11}}{2}\left[\frac{P^2}{Ah}+\frac{M^2}{Ih^3}+2\frac{PM}{\sqrt{AIh^2}}\sin\gamma\right]. \tag{10}$$

The geometric factors are given by

$$\frac{1}{A}=1+4\eta+6\eta^2+3\eta^3,\ \frac{1}{I}=12(1+\eta^3),\ \frac{\sin\gamma}{\sqrt{AI}}=6\eta^2(1+\eta) \tag{11}$$

where the angle γ is restricted to $|\gamma|<\pi/2$ for definiteness. Without loss of generality, attention will be restricted to $h\le H$, or equivalently, $0\le\eta\le1$. The energy release rate given by equations (10) and (11) is valid even if the material is generally anisotropic.

As shown in Appendix A, for the problem in Figs. 1(*a*) and 1(*c*), the combinations $\lambda^{-3/8}K_I$ and $\lambda^{-1/8}K_{II}$ are independent of λ. It will be obvious immediately that this fact simplifies

Table 2 $\omega(\eta, \rho)$ (in degrees)

η \ ρ	−5	0	1	2	3	4
0	51.0	51.7	52.1	52.2	52.2	52.3
0.5	50.4	50.4	50.9	51.1	51.1	51.7
1	49.1	49.1	49.1	49.1	49.1	49.1

the problem significantly. Equating the two energy release rate expressions (8) and (10), one can verify

$$\sqrt{n}\,|\lambda^{-3/8}K_I + i\lambda^{-1/8}K_{II}| = \frac{1}{\sqrt{2}}\left|\frac{P}{\sqrt{hA}} - ie^{i\gamma}\frac{M}{\sqrt{h^3 I}}\right| \tag{12}$$

where $i=\sqrt{-1}$ and $|a|$ stands for the magnitude of a complex number a. Equation (12) states that two complex quantities have the same magnitude. Consequently, they can differ only by a phase angle shift, designated as ω, namely,

$$\left(\sqrt{n}(\lambda^{-3/8}K_I + i\lambda^{-1/8}K_{II}) = \frac{e^{i\omega}}{\sqrt{2}}\frac{P}{\sqrt{hA}} - ie^{i\gamma}\frac{M}{\sqrt{h^3 I}}\right). \tag{13}$$

On dimensional grounds, ω should be nondimensional function of nondimensional quantities Ph/M, η, λ, and ρ. However, by linearity, ω should not depend on Ph/M; nor should it depend on λ, since both sides of equation (13) are independent of λ. Therefore, the angle ω depends on η and ρ only, i.e.,

$$\omega = \omega(\eta, \rho). \tag{14}$$

Rewrite equation (13) more explicitly as

$$K_I = \frac{\lambda^{3/8}}{\sqrt{2n}}\left[\frac{P}{\sqrt{hA}}\cos\omega + \frac{M}{\sqrt{h^3 I}}\sin(\omega+\gamma)\right]$$
$$K_{II} = \frac{\lambda^{1/8}}{\sqrt{2n}}\left[\frac{P}{\sqrt{hA}}\sin\omega - \frac{M}{\sqrt{h^3 I}}\cos(\omega+\gamma)\right] \tag{15}$$

so that the stress intensity factors are fully determined apart from the single dimensionless real function $\omega(\eta, \rho)$. From equation (15) one can restrict ω in the range $0<\omega<\pi/2$ to recover the positive signs of K_I and K_{II} anticipated for the special case $P>0$ but $M=0$.

Specific determination of the function $\omega(\eta, \rho)$ requires that the crack problem in Fig. 1(*c*) be solved *rigorously* for a given pair (η, ρ), for an arbitrary set of values of λ, h, P, and M. We will show next that ω is around 50 deg. Some early works on partitioning mixed-mode stress intensity factors from the energy release rate were based on unjustified symmetry arguments and contains significant errors (e.g., Tada et al., 1985, pp. 29.2, 29.4, 29.9 and Williams, 1988, Fig. 10(*a*)). In the following, an exact solution for ω is found for the case $h=H$, or $\eta=1$. Numerical solutions are presented for other cases, and a simple estimate is given for practical applications.

(i) $\omega(1, \rho)$. Exact solution can be obtained for this case by considering a special loading $P=0$, $M=1$. The geometric factors in equations (9) and (11) for $\eta=1$ are

$$A=\frac{1}{14},\ I=\frac{1}{24},\ \sin\gamma=\sqrt{\frac{3}{7}}$$
$$C_1=\frac{1}{2},\ C_2=\frac{3}{4},\ C_3=\frac{1}{8}. \tag{16}$$

Notice that $K_{II}=0$ due to the symmetry, which, when substituted into equation (15), gives $\cos(\omega+\gamma)=0$. Thus, $\omega=\cos^{-1}\sqrt{(3/7)}\approx 49.1$ deg. It is revealing that $\omega(1, \rho)$ does *not* depend on ρ. This indicates that the function $\omega(\eta, \rho)$ may vary weakly with ρ even if $\eta\neq 1$.

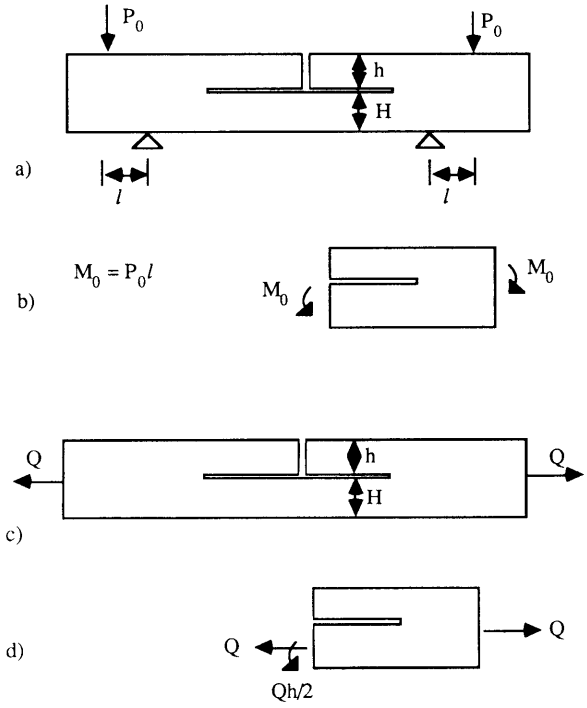

Fig. 2 Transverse splitting from notches; (*a*) four-point bend specimen, (*b*) equivalent bend moment, (*c*) delamination specimen, and (*d*) equivalent load for the delamination specimen

(ii) $\omega(\eta, 1)$. This case is equivalent to the isotropic version of the same problem, which has been solved by Suo and Hutchinson (1988a, b). For $0\leq\eta\leq 1$, an excellent approximation is

$$\omega = 52.1 - 3\eta, \quad \text{in degrees.} \tag{17}$$

(iii) $\omega(\eta, \rho)$. An integral equation is formulated and solved numerically in Appendix B for the general case. The extracted values of ω are listed in Table 2. One notes immediately that ω is a very weak function of ρ. This implies that equation (17) is an adequate estimate for a wide range of ρ for $0\leq\eta\leq 1$.

3 Fracture Specimens

3.1 A Four-Point Bend Specimen. The specimen illustrated in Fig. 2(*a*) is considered first. The beam is cut from an orthotropic material, with its principal axes coincident with the material principal axes. When the crack is long compared with h, but still lying within the central region of the specimen, the specimen can be well approximated by the system in Fig. 2(*b*). It has been shown by finite element calculations (Charalambides et al., 1989) for an analogous specimen that the crack-tip field is indifferent to the crack length if it is sufficiently long. Consequently, the structure in Fig. 2(*b*) can be imagined to be infinitely long in the crack direction. This falls into the class of the problems (Fig. 2(*a*)) analyzed in the previous section, with the special loading combination

$$P_1 = M_1 = P_3 = 0,\ M_3 = -M_0. \tag{18}$$

The equivalent loads controlling the singular field are calculated from equation (9), i.e.,

$$P = C_2 M_0/h,\ M = C_3 M_0. \tag{19}$$

The stress intensity factors are obtained when the above are substituted into equation (15), that is

$$K_I=\frac{\lambda^{3/8}}{\sqrt{2n}}M_0h^{-3/2}[C_2A^{-1/2}\cos\omega+C_3I^{-1/2}\sin(\omega+\gamma)]$$
$$K_{II}=\frac{\lambda^{1/8}}{\sqrt{2n}}M_0h^{-3/2}[C_2A^{-1/2}\sin\omega-C_3I^{-1/2}\cos(\omega+\gamma)] \quad (20)$$

where ω can be approximated by equation (17). For the special case $h=H$, or $\eta=1$, $\omega+\gamma=\pi/2$, $\cos\omega=\sqrt{(3/7)}$, $\sin\omega=\sqrt{(4/7)}$, with various geometric factors given in equation (16), equation (20) can be specialized to

$$K_I=\sqrt{3}\lambda^{3/8}n^{-1/2}M_0h^{-3/2},\ K_{II}=\frac{3}{2}\lambda^{1/8}n^{-1/2}M_0h^{-3/2}. \quad (21)$$

This is an exact solution. Notice that from equation (21),

$$\frac{K_{II}}{K_I}=\frac{\sqrt{3}}{2}\lambda^{-1/4}. \quad (21a)$$

Equation (21*a*) indicates that mode I and mode II stress intensity factors are comparable for this test arrangement.

3.2 A Tensile Specimen. Parallel results for the same geometry under tension (Fig. 2(*c*), (*d*)) are listed as follows. The stress intensity factors are given by

$$K_I=\frac{\lambda^{3/8}}{\sqrt{2n}}Qh^{-1/2}C_1A^{-1/2}\cos\omega$$
$$K_{II}=\frac{\lambda^{1/8}}{\sqrt{2n}}Qh^{-1/2}C_1A^{-1/2}\sin\omega \quad (22)$$

where, for an arbitrary value of $\eta=h/H$, C_1 and A are defined in equations (9) and (11), and ω can be approximated by equation (17). The solution for the case $h=H$, or $\eta=1$, is exact, which is

$$K_I=\frac{\sqrt{3}}{2}\lambda^{3/8}n^{-1/2}h^{-1/2}Q,\ K_{II}=\lambda^{1/2}n^{-1/2}h^{-1/2}Q, \quad (23)$$

thereby the ratio K_{II}/K_I, for the case $h=H$, is given by

$$\frac{K_{II}}{K_I}=\frac{2}{\sqrt{3}}\lambda^{-1/4}. \quad (23a)$$

Again, there is a comparable amount of stress intensity of the two modes.

3.3 More Specimens. Illustrated in Fig. 3 are geometries utilized predominantly in composite and wood fracture testing. The specimens are cut from bulk materials with principal material axes aligned with specimen axes. A common feature for all these specimens is that no specific length scale is involved in one direction. With such specimens, it has generally been the practice to use the stress intensity factors determined for the corresponding isotropic specimens (e.g., Ashby et al., 1985, Michalske and Hellmann, 1988). This can be easily justified as follows: The stress intensity factors, in general, depend on the two anisotropy measures, λ and ρ. Exploiting the rescaling technique outlined in Appendix A one can confirm that, for all configurations in Fig. 3, the stress intensity factors are independent of λ. Given the fact that ρ is typically in the range between 0 and 5, and that the solutions for analogous problems only weakly depend on ρ, one can reasonably expect that the stress intensity factors are *almost* independent of ρ. Consequently, the stress intensity factors for these geometries are nearly independent of any anisotropic factors, and thus the use of solutions for isotropic materials should be appropriate. Evidently unaware of the roles played by λ and ρ, Sweeny (1988) carried out a numerical analysis for an edge crack in an orthotropic half plane (Fig. 3(*a*)). The Table 1 in his paper can be reduced concisely as

$$K_I=Y\sigma\sqrt{\pi a},\ Y=1.12-0.011(\rho-1),\quad \text{for } 1<\rho<8. \quad (24)$$

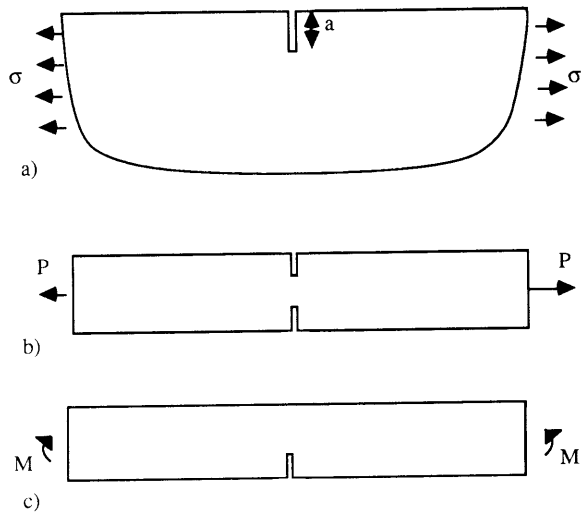

Fig. 3 Several conventional fracture specimens

The rescaling concepts have been extended to tackle specimens of finite geometries. Insights thus gained and a user-friendly catalog of most commonly used orthotropic specimens are reported in Suo et al. (1990) and Bao et al. (1990).

4 Extension to an Anisotropic Strip

Arguments leading to the stress intensity factor expression (15) have been used successfully in various contexts by Thouless et al. (1987), Hutchinson et al. (1988), Drory et al. (1988), and Suo and Hutchinson (1989a,b,c). The generality may be appreciated by considering the problem with the same configuration as Fig. 1(*c*), but with a generally anisotropic material replacing the orthotropic material considered earlier. The Sih-Paris-Irwin energy release rate expression can be rearranged as

$$G=b_{11}(n_1\lambda^{-3/4}K_I^2+n_2\lambda^{-1/4}K_{II}^2$$
$$+2\sqrt{n_1n_2}\lambda^{-1/2}K_IK_{II}\sin\nu). \quad (25)$$

Here, n_1, n_2, and ν can be extracted from the work by Sih et al. (1965) as

$$n_1=-\frac{1}{2}\mathrm{Im}[t_1^{-1}+t_2^{-1}],\ n_2=\frac{1}{2}\mathrm{Im}[t_1+t_2],\ \sqrt{n_1n_2}\sin\nu=\frac{1}{2}\mathrm{Im}[t_1t_2] \quad (26)$$

and t_1 and t_2 are roots with positive imaginary parts of

$$t^4-2\rho_1t^3+2\rho t^2-2\rho_2t+1=0 \quad (27)$$

where ρ_1 and ρ_2 are defined in Appendix A. Comparing equation (25) with equation (10) one obtains

$$\left|\sqrt{n_1}\lambda^{-3/8}K_I+ie^{-i\nu}\sqrt{n_2}\lambda^{-1/8}K_{II}\right|$$
$$=\frac{1}{\sqrt{2}}\left|\frac{P}{\sqrt{hA}}-ie^{i\gamma}\frac{M}{\sqrt{h^3I}}\right| \quad (28)$$

where A and I are defined by equation (11). Again one can introduce a phase angle shift $\omega=\omega(\eta,\ \rho,\ \rho_1,\ \rho_2)$, such that

$$\sqrt{n_1}\lambda^{-3/8}K_I+ie^{-i\nu}\sqrt{n_2}\lambda^{-1/8}K_{II}$$
$$=\frac{e^{i\omega}}{\sqrt{2}}\left(\frac{P}{\sqrt{hA}}-ie^{i\gamma}\frac{M}{\sqrt{h^3I}}\right). \quad (29)$$

Consequently, the stress intensity factors K_I and K_{II} are fully determined apart from the function ω. One may anticipate the

approximation equation (17) to be valid for wide ranges of ρ, ρ_1, and ρ_2.

It is not a very difficult exercise to derive a formula analogous to equation (26) for an interface crack between two layers of dissimilar anisotropic materials, so that such interesting problems as bicrystal specimens (e.g., Wang, 1988) and interlaminar fracture in composites can be addressed. Helpful hints may be found in Suo and Hutchinson (1990). The corresponding relation between energy release rate and stress intensity factors can be found in Suo (1990).

Acknowledgments

The author is very grateful to A. G. Evans and J. W. Hutchinson for suggesting this problem and potential applications. This work was supported in part by DARPA University Research Initiative (Subagreement P.O. No. VB38639-0 with the University of California, Santa Barbara, ONR Prime Contract N00014-86-k-0753), by the National Science Foundation under Grant MSM-88-12779, and by the Division of Applied Sciences, Harvard University.

References

Argon, A. S., Gupta, V., Landis, H. S., and Cornie, J. A., 1989, "Intrinsic Toughness of Interfaces Between SiC Coatings and Substrates of Si or C Fibers," *J. Mater. Sci.*, Vol. 24, p. 1406-1412.

Ashby, M. F., Easterling, K. E., Harrysson, R., and Maiti, S. K., 1985, "The Fracture and Toughness of Woods," *Proc. Roy. Soc. Lond.*, Vol. A398, pp. 261-280.

Bao, G., Ho, S., Fan, B., and Suo, Z., 1990, "Orthotropy Rescaling and Fracture Specimens for Composite Materials," manuscript in preparation.

Budiansky, B., Hutchinson, J. W. and Evans, A. G., 1986, "Matrix Fracture in Fibre-reinforced Ceramics," *J. Mech. Phys. Solids*, Vol. 34, pp. 167-189.

Chai, H., 1988, "Shear Fracture," *Int. J. Fracture*, Vol. 37, pp. 137-159.

Charalambides, P. G., Lund, J., Evans, A. G., and McMeeking, R. M., 1989, "A Test Specimen for Determining the Fracture Resistance of Bimaterial Interfaces," ASME JOURNAL OF APPLIED MECHANICS, Vol. 56, pp. 77-82.

Drory, M. D., Thouless, M. D., and Evans, A. G. 1988, "The Cracking and Decohesion of Thin Films," *Acta Met.*, Vol. 36, pp. 2019-2028.

Hutchinson, J. W., Mear, M. E., and Rice, J. R., 1987, "Crack Paralleling an Interface between Dissimilar Materials," ASME JOURNAL OF APPLIED MECHANICS, Vol. 54, pp. 828-832.

Lekhnitskii, S. G., 1963, *Theory of Elasticity of an Anisotropic Body*, Holden-Day, Inc.

Liechti, K. M., and Hanson, E. C., 1988, "Nonlinear Effects in Mixed-Mode Interfacial Delamination," *Int. J. Fract.*, Vol. 36, pp. 199-217.

Marshall, D. B., and Evans, A. G., 1985, "Failure Mechanism in Ceramic-Fiber/Ceramic-Matrix Composites," *J. Am. Ceram. Soc.*, Vol. 68, pp. 225-231.

Michalske, T. A., and Hellmann, J. R., 1988, "Strength and Toughness of Continuous-Alumina-Fiber-Reinforced Glass-Matrix Composites," *J. Am. Ceram. Soc.*, Vol. 71, pp. 725-731.

Prewo, K. M., 1986, "Tension and Flexural Strength of Silicon Carbide Fiber-Reinforced Glass Ceramics," *J. Matter. Sci.*, Vol. 21, pp. 3590-3600.

Rice, J. R., 1968, "Mathematical Analysis in the Mechanics of Fracture," *Fracture, an Advanced Treatise*, Vol. 2, H. Liebowitz, ed., Academic Press, New York, pp. 191-311.

Sbaizero, O., Charalambides, P. G., and Evans, A. G., 1988, "Delamination Cracking in a Laminated Ceramic Matrix Composite," *Acta Met*, in press.

Sih, G. C., Paris, P. C., and Irwin, G. R., 1965, "On Cracks in Rectilinearly Anisotropic Bodies," *Int. J. Fracture Mech.*, Vol. 1, pp. 189-203.

Suo, Z., 1990, "Singularities, Interfaces and Cracks in Dissimilar Anistropic Media," *Proc. R. Soc. Lond.*, Vol. A427, pp. 331-358.

Suo, Z., and Hutchinson, J. W., 1990, "Interface Crack Between Two Elastic Layers," *Int. J. Fract.*, Vol. 43, pp. 1-18.

Suo, Z., and Hutchinson, J. W., 1989a, "Steady-state Cracking in Brittle Substrate beneath Adherent Films," *Int. J. Solids Structures*, Vol. 25, pp. 1337-1353.

Suo, Z., and Hutchinson, J. W., 1989b, "Sandwich Test Specimens for Measuring Interface Crack Toughness," *Mat. Sci. Eng.*, Vol. A107, pp. 135-143.

Suo, Z., Bao, G., Fan, B., and Wang, T. C., 1990, "Orthotropy Rescaling and Implications for Fracture in Composites," submitted for publication.

Sweeney, J., 1988, "The Stress Intensity for an Edge Crack in a Semi-infinite Orthotropic Body," *Int. J. Fract.*, Vol. 37, pp. 233-241.

Tada, H., Paris, P. C., and Irwin, G. R. 1985, *The Stress Analysis of Cracks Handbook*, Del Research, St. Louis, MO.

Thouless, M. D., Evans, A. G., Ashby, M. F., and Hutchinson, J. W., 1987, "The Edge Cracking and Spalling of Brittle Plates," *Acta Met.*, Vol. 35, pp. 1333-1341.

Wang, J.-S., 1988, "A New Type of Brittle Fracture in an FCC Metal Bicrystal with Intergranular Segregation," *J. Matter. Res.*, Vol. 3, pp. 16-28.

Wang, J.-S., and Suo, Z., 1990, "Experimental Determination of Interfacial Toughness Curves Using Brazil Nut Sandwiches," *Acta Met.*, in press.

Williams, J. G., 1988, "On the Calculation of Energy Release Rates for Cracked Laminates," *Int. J. Fract.*, Vol. 36, pp. 101-119.

Wu, E. M., 1967, "Application of Fracture Mechanics to Anisotropic Plates," ASME JOURNAL OF APPLIED MECHANICS, Vol. 34, pp. 967-974.

APPENDIX A

Orthotropy Rescaling

Let $U(x, y)$ by the Airy stress function, namely,

$$\sigma_x=\frac{\partial^2 U}{\partial y^2},\ \sigma_y=\frac{\partial^2 U}{\partial x^2},\ \tau_{xy}=-\frac{\partial^2 U}{\partial x\partial y}. \tag{A1}$$

The differential equation of $U(x, y)$ for rectilinearly anisotropic materials is obtained from the compatibility equation (cf. Lekhnitskii, 1963)

$$\frac{\partial^4 U}{\partial x^4}-2\rho_2\lambda^{1/4}\frac{\partial^4 U}{\partial x^3\partial y}+2\rho\lambda^{1/2}\frac{\partial^4 U}{\partial x^2\partial y^2}-2\rho_1\lambda^{3/4}\frac{\partial^4 U}{\partial x\partial y^3}+\lambda\frac{\partial^4 U}{\partial y^4}=0 \tag{A2}$$

where λ and ρ are defined in the body of the paper and $\rho_1\lambda^{3/4}=b_{16}/b_{22}$, $\rho_2\lambda^{1/4}=b_{26}/b_{22}$. Now it is obvious that for any simply connected domain of anisotropic medium with traction prescribed on its boundary, the stresses should only depend on four (rather than five) nondimensional elastic parameters. If the material is orthotropic with the principal axes in the x and y-directions, $\rho_1=\rho_2=0$, the stresses should only depend on two parameters λ and ρ. Moreover, for the problem in Fig. 2(a) with no specific length scale in x-direction, we are able to show explicitly the way in which stress intensity factors depend on λ. Rescale the x-axis by

$$\xi=\lambda^{1/4}x. \tag{A3}$$

The boundary value problem in Fig. 2(a) is then governed by the following differential equation

$$\frac{\partial^4 U}{\partial \xi^4}-2\rho_2\frac{\partial^4 U}{\partial \xi^3\partial y}+2\rho\frac{\partial^4 U}{\partial \xi^2\partial y^2}-2\rho_1\frac{\partial^4 U}{\partial \xi\partial y^3}+\frac{\partial^4 U}{\partial y^4}=0 \tag{A4}$$

and boundary conditions on (ξ, y) plane

$$\frac{\partial^2 U}{\partial y\partial \xi}=0,\ \frac{\partial^2 U}{\partial y^2}=\text{prescribed traction},\ \xi\to\pm\infty,\ -H<y<h \tag{A5}$$

$$\frac{\partial^2 U}{\partial \xi^2}=\frac{\partial^2 U}{\partial \xi\partial y}=0,\ \xi<0,\ y=0;\ -\infty<\xi<\infty,\ y=-H,\ h.$$

Clearly, $U(\xi, y)$ will not depend explicitly on λ. This has very strong implications as the stress intensity factors K_I and K_{II} are calculated

$$K_I=\lim_{x\to 0}\sqrt{2\pi x}\sigma_y(x, 0)=\lambda^{3/8}\lim_{\xi\to 0}\sqrt{2\pi\xi}\,\frac{\partial^2 U(\xi, 0)}{\partial \xi^2} \tag{A6}$$

$$K_{II}=\lim_{x\to 0}\sqrt{2\pi x}\tau_{xy}(x, 0)=-\lambda^{1/8}\lim_{\xi\to 0}\sqrt{2\pi\xi}\frac{\partial^2 U(\xi, 0)}{\partial \xi\partial y} \tag{A7}$$

so that the combinations $\lambda^{-3/8}K_I$ and $\lambda^{-1/8}K_{II}$ are independent of λ.

APPENDIX B

Integral Equation Formulation

An integral equation for the plane elasticity problem of Fig. 2(c) is formulated based on the dislocation solutions developed in Appendix C. Since only the function $\omega(\eta, \rho)$ is to be extracted from the numerical solution, one can take

$$\lambda=1,\ h=1,\ P=1,\ b_{11}=1, \tag{B1}$$

and M will be specified shortly to simplify the numerical analysis.

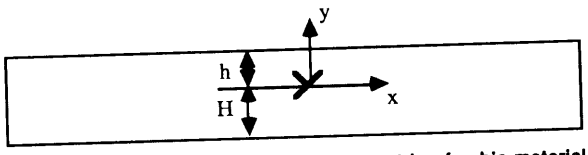

Fig. 4 An edge dislocation in an infinite strip of cubic material

The semi-infinite crack is simulated by an array of continuously distributed edge dislocations along the negative x-axis, with components $b_\alpha(\xi)$ at $x=\xi$. The traction-free condition along the crack faces results in the integral equations

$$\int_{-\infty}^{0} \frac{2B_\alpha(\xi)}{x-\xi} d\xi + \int_{-\infty}^{0} F_{\alpha\beta}(x-\xi) B_\beta(\xi) d\xi = 0, \text{ for } -\infty < x < 0 \quad \text{(B2)}$$

where the first integral is in the Cauchy principal value sense, and the convention of summing up a repeated Greek suffix is adopted. Here,

$$B_\alpha(\xi) = \frac{1}{8\pi n} b_\alpha(\xi), \; n = \sqrt{\frac{\rho+1}{2}}. \quad \text{(B3)}$$

The kernel functions $F_{\alpha\beta}(\zeta)$ are given in Appendix C; they are well behaved in the whole range $-\infty < \zeta < +\infty$, with asymptotes

$$F_{\alpha\beta}(\zeta) = -\frac{2}{\zeta}\delta_{\alpha\beta} + O\left(\frac{1}{\zeta^3}\right) \quad \text{as } \zeta \to \infty. \quad \text{(B4)}$$

Noticing that by definition the Burgers vector, b_α, is related to the crack face relative displacement, δ_α, by

$$b_\alpha(x) = -\frac{\partial}{\partial x}\delta_\alpha(x), \quad \text{(B5)}$$

one can verify the following asymptotic behaviors for $B_\alpha(\xi)$

$$B_1(\xi) = (2\pi)^{-3/2}\frac{K_{II}}{\sqrt{-\xi}}, \; B_2(\xi) = (2\pi)^{-3/2}\frac{K_I}{\sqrt{-\xi}} \quad \text{(B6)}$$

as $\xi \to 0^-$, and

$$B_1(\xi) = \frac{1}{8\pi n}[1+\eta(4+3\eta) - 6M(1-\eta^2)], \; B_2(\xi) = \text{constant}$$

$$M = -\sqrt{\frac{I}{A}}\sin\gamma \quad \text{(B7)}$$

as $\xi \to -\infty$, where M has been chosen such that $B_2(-\infty)$ remains finite. And K_I, K_{II} and the "constant" in (B7) are not known *a priori*, but must be determined as part of the solution to the integral equations. The integral equations, together with the specified asymptotes, constitute a well-posed mathematical problem for the unknown distributions $B_\alpha(\xi)$. The details of the numerical solution procedure for analogous problems can be found in Thouless et al. (1987), and Suo and Hutchinson (1989a).

Once the $B_\alpha(\xi)$ are obtained for a given pair η and ρ, the stress intensity factors are evaluated from equation (B6). The function $\omega(\eta, \rho)$ is then extracted by specializing equation (13) with (B1), (B7) to

$$K_I + iK_{II} = \frac{\cos\gamma}{\sqrt{2nA}} e^{i(\omega+\gamma)}. \quad \text{(B8)}$$

The numerical solution yields both K_I and K_{II} and each results in a value of ω. This provides a consistency check on the accuracy of the solution. For example, knowing K_I and K_{II}, one can calculate $\cos(\omega+\gamma)$ and $\sin(\omega+\gamma)$ independently from equation (B8), and hence the check can be chosen as $[\cos^2(\omega+\gamma) + \sin^2(\omega+\gamma)]^{1/2} - 1$. The results reported in Table 2 were computed with the consistency check satisfied to better than 0.1 percent. It is believed that the accuracy of ω is comparable.

APPENDIX C

An Edge Dislocation in Anisotropic Structures

In Appendix B, the solution of an edge dislocation embedded in a strip of cubic material (Fig. 4) is used as the kernel of the integral equation. This solution, together with analytic solutions to a dislocation in an infinite and semi-infinite space of generally anisotropic material, is constructed in this Appendix.

It has been shown in Lekhnitskii (1963) that the problems of plane anistropic elasticity can be conveniently formulated in terms of two analytic functions, $\phi_1(z_1)$ and $\phi_2(z_2)$ with two complex variables, $z_j = x + \mu_j y$. The parameters μ_1 and μ_2 are solved from the algebraic equation

$$b_{11}\mu^4 - 2b_{16}\mu^3 + (2b_{12}+b_{66})\mu^2 - 2b_{26}\mu + b_{22} = 0. \quad \text{(C1)}$$

The roots of equation (1) can never be real, and thus they occur in conjugate pairs. Here μ_1 and μ_2 are chosen to be the ones with positive imaginary parts. The stresses, resultant forces on an arc and displacements are given by

$$\begin{aligned}
\sigma_x &= 2\text{Re}[\mu_1^2\phi_1'(z_1) + \mu_2^2\phi_2'(z_2)] \\
\sigma_y &= 2\text{Re}[\phi_1'(z_1) + \phi_2'(z_2)] \\
\tau_{xy} &= -2\text{Re}[\mu_1\phi_1'(z_1) + \mu_2\phi_2'(z_2)] \\
f_x &= 2\text{Re}[\mu_1\phi_1(z_1) + \mu_2\phi_2(z_2)] \\
f_y &= -2\text{Re}[\phi_1(z_1) + \phi_2(z_2)] \\
u_x &= 2\text{Re}[p_1\phi(z_1) + p_2\phi_2(z_2)] \\
u_y &= 2\text{Re}[q_1\phi_1(z_1) + q_2\phi_2(z_2)]
\end{aligned} \quad \text{(C2)}$$

where Re[ ] signifies the real part of a complex quantity, and

$$p_j = b_{11}\mu_j^2 + b_{12} - b_{16}\mu_j, \; q_j = b_{22}/\mu_j + b_{12}\mu_j - b_{26}. \quad \text{(C3)}$$

(i) An Isolated Dislocation in an Infinite Body

The potentials for an edge dislocation with Burgers vector b_x and b_y at the point (x_0, y_0) in an infinite body are of the form

$$\phi_{j0}(z) = W_j \ln(z - s_j), \; s_j = x_0 + \mu_j y_0 \quad \text{(C4)}$$

where the suffix 0 attached to the potentials indicates that the solution is for an *infinite body*. The complex constants W_1 and W_2 are determined from

$$\begin{cases}
\text{Im}[W_1 + W_2] = 0 \\
\text{Im}[\mu_1 W_1 + \mu_2 W_2] = 0 \\
\text{Im}[\mu_1^2 W_1 + \mu_2^2 W_2] = -b_x/(4\pi b_{11}) \\
\text{Im}[W_1/\mu_1 + W_2/\mu_2] = -b_y/(4\pi b_{22})
\end{cases} \quad \text{(C5)}$$

where Im[ ] represents the imaginary part of a quantity. For the special case that the material is cubic with the principal axes along the x and y-axes, equation (C5) yields

$$W_1 = \frac{1}{\mu_1 - \mu_2}[-B_x + B_y/\mu_1], \; W_2 = \frac{1}{\mu_1 - \mu_2}[B_x - B_y/\mu_2]$$

$$B_\alpha = \frac{b_\alpha}{8\pi n b_{11}}. \quad \text{(C6)}$$

Specializing equation (C1) to a cubic material ($b_{16}=b_{26}=0$, $b_{11}=b_{22}$) gives

$$\mu_1=i(n+m),\quad \mu_2=i(n-m),\quad \text{for } 1<\rho<\infty$$
$$\mu_1=in+m,\quad \mu_2=in-m,\quad \text{for } -1<\rho<1 \tag{C7}$$
$$n=\sqrt{\frac{1+\rho}{2}},\quad m=\sqrt{\left|\frac{1-\rho}{2}\right|}\ .$$

The degenerate value $\rho=1$ (corresponding to isotropic materials) can be treated as the limiting case. With the dislocation at the origin, i.e., $x_0=y_0=0$, the stresses are

$$\sigma^0_{\alpha\beta}(x,y)=f_{\alpha\beta\gamma}B_\gamma,\ f_{\alpha\beta\gamma}=\frac{1}{m}[g_{\alpha\beta\gamma}(m)-g_{\alpha\beta\gamma}(-m)] \tag{C8}$$

where

$$g_{111}(m)=-\frac{(n+m)^3y}{r^2},\ g_{112}(m)=g_{121}(m)=\frac{(n+m)x}{r^2}$$
$$g_{222}(m)=-\frac{y/(n+m)}{r^2},\ g_{221}(m)=g_{122}(m)=\frac{(n+m)y}{r^2} \tag{C9}$$
$$r^2=x^2+(n+m)^2y^2$$

for $\rho>1$, and

$$g_{111}(m)=\frac{\rho x-my}{r^2},\ g_{112}(m)=g_{121}(m)=\frac{mx+y}{r^2}$$
$$g_{222}(m)=\frac{mx-\rho y}{r^2},\ g_{221}(m)=g_{122}(m)=-\frac{x+my}{r^2} \tag{C10}$$
$$r^2=(x+my)^2+(ny)^2$$

for $-1<\rho<1$.

(ii) A Dislocation in Half Space

For a line singularity, such as a dislocation and line force, in generally anisotropic half space with traction-free boundary $y=0$, it has been shown by Suo (1990) that the potentials can be constructed with the solutions for the same singularity in an infinite body, namely,

$$\phi_1(z)=\phi_{10}(z)+\frac{1}{\mu_1-\mu_2}[(\mu_2-\bar{\mu}_1)\bar{\phi}_{10}(z)+(\mu_2-\bar{\mu}_2)\bar{\phi}_{20}(z)] \tag{C11}$$
$$\phi_2(z)=\phi_{20}(z)+\frac{1}{\mu_1-\mu_2}[(\bar{\mu}_1-\mu_1)\bar{\phi}_{10}(z)+(\bar{\mu}_2-\mu_1)\bar{\phi}_{20}(z)].$$

(iii) A Dislocation in an Infinite Layer

A superposition scheme is used here to construct the solution for an edge dislocation embedded in an infinite strip (Fig. 4). Attention will be confined to cubic materials with a principal axis along the direction of the strip. A solution without singularity in the strip, which is represented by the Airy stress function $U(x, y)$ in Appendix A, is superposed onto the solution to an edge dislocation in an infinite body to nullify the traction on the strip boundaries. The following conventions of the Fourier-cos and -sin transforms for even and odd functions, respectively, will be adopted

$$f(x)=\int_0^{+\infty}\hat{f}(\theta)\cos\theta x\,d\theta,\ \hat{f}(\theta)=\frac{2}{\pi}\int_0^{+\infty}f(x)\cos\theta x\,dx$$
$$g(x)=\int_0^{+\infty}\hat{g}(\theta)\sin\theta x\,d\theta,\ \hat{g}(\theta)=\frac{2}{\pi}\int_0^{+\infty}g(x)\sin\theta x\,dx. \tag{C12}$$

Owing to the symmetry of the configuration, the stress function can be expressed by the Fourier integrals

$$U(x,y)=B_x\int_0^\infty\{\hat{U}_i(\theta,y)\}^T\{A_i(\theta)\}\frac{\cos\theta x}{\theta^2}d\theta$$
$$+B_y\int_0^\infty\{\hat{U}_i(\theta,y)\}^T\{C_i(\theta)\}\frac{\sin\theta x}{\theta^2}d\theta \tag{C13}$$

where $\hat{U}$'s are solved from

$$\left[\theta^4-2\rho\theta^2\frac{\partial^2}{\partial y^2}+\frac{\partial^4}{\partial y^4}\right]\hat{U}(\theta,y)=0. \tag{C14}$$

The solutions are

$$\{\hat{U}_i(\theta,y)\}^T=$$
$$\begin{cases}\{e^{(n+m)y\theta},\ e^{(n-m)y\theta},\ e^{(-n-m)y\theta},\ e^{(-n+m)y\theta}\},\ \rho>1\\ \{e^{ny\theta}\sin(my\theta),\ e^{ny\theta}\cos(my\theta),\ e^{-ny\theta}\sin(my\theta),\ e^{-ny\theta}\cos(my\theta)\},\\ \qquad -1<\rho<1\\ \{e^{y\theta},\ y\theta e^{y\theta},\ e^{-y\theta}y\theta,\ e^{-y\theta}\},\ \rho=1\end{cases} \tag{C15}$$

The stresses are derived from equation (A1).

$$\sigma_{yy}(x,y)=-B_x\int_0^\infty\{\hat{U}_i(\theta,y)\}^T\{A_i(\theta)\}\cos\theta x\,d\theta$$
$$-B_y\int_0^\infty\{\hat{U}_i(\theta,y)\}^T\{C_i(\theta)\}\sin\theta x\,d\theta \tag{C16a}$$

and

$$\tau_{xy}(x,y)=+B_x\int_0^\infty\{\partial\hat{U}_i(\theta,y)/\partial y\}^T\{A_i(\theta)\}\sin\theta x\,d\theta$$
$$-B_y\int_0^\infty\{\partial\hat{U}_i(\theta,y)/\partial y\}^T\{C_i(\theta)\}\cos\theta x\,d\theta. \tag{C16b}$$

The coefficients A's and C's are used to satisfy the strip boundary conditions. Written in the Fourier transform variables, these conditions become

$$\begin{bmatrix}\{\hat{U}_i(h)\}^T\\ \{\partial\hat{U}_i(h)/\partial y\}^T\\ \{\hat{U}_i(-H)\}^T\\ \{\partial\hat{U}_i(-H)/\partial y\}^T\end{bmatrix}\begin{bmatrix}A_1 & C_1\\ A_2 & C_2\\ A_3 & C_3\\ A_4 & C_4\end{bmatrix}=$$
$$\begin{bmatrix}\hat{f}_{221}(h) & \hat{f}_{222}(h)\\ -\hat{f}_{121}(h) & \hat{f}_{122}(h)\\ \hat{f}_{221}(-H) & \hat{f}_{222}(-H)\\ -\hat{f}_{121}(-H) & \hat{f}_{122}(-H)\end{bmatrix} \tag{C17}$$

where the Fourier transforms of the functions defined in equations (C8)–(C10) are

$$\hat{f}_{121}(y)=\frac{1}{m}[(n+m)e^{-(n+m)|y|\theta}-(n-m)e^{-(n-m)|y|\theta}]$$
$$\hat{f}_{222}(y)=\frac{1}{m}\left[-\frac{1}{n+m}e^{-(n+m)|y|\theta}+\frac{1}{n-m}e^{-(n-m)|y|\theta}\right] \tag{C18}$$
$$\hat{f}_{221}(y)=\hat{f}_{122}(y)=\frac{\mathrm{sgn}(y)}{m}[e^{-(n+m)|y|\theta}-e^{-(n-m)|y|\theta}]$$

for $\rho>1$, and

$$\hat{f}_{121}(y)=2\left[\cos(my\theta)-n\frac{\sin(m|y|\theta}{m}\right]e^{-n|y|\theta}$$
$$\hat{f}_{222}(y)=2\left[\cos(my\theta)+n\frac{\sin(m|y|\theta)}{m}\right]e^{-n|y|\theta} \tag{C19}$$
$$\hat{f}_{221}(y)=\hat{f}_{122}(y)=-2\left[\frac{\sin(my\theta)}{m}\right]e^{-n|y|\theta}$$

for $-1<\rho<1$. The dependence on θ has not been noted explicitly.

In the integral equation formulation in Appendix B, the stresses at x induced by the dislocation at $x=0$ are desired along the line parallel to the strip boundaries with the dislocation on it. They can be written in the form

$$\sigma_{2\alpha}(x)=\frac{2B_\alpha}{x}+F_{\alpha\beta}(x)B_\beta \tag{C20}$$

where F's are to be evaluated numerically using the Fourier integrals equation (C16) letting $y=0$. However, for the half plane problem, i.e, $H\to\infty$, analytic expressions are obtained from equation (C11). The results are

$$F_{\alpha\beta}=\left(\frac{n}{m}\right)^2[D_{\alpha\beta}(m)+D_{\alpha\beta}(-m)-2D_{\alpha\beta}(0)/n^2],\ \alpha=\beta \tag{C21}$$

$$F_{\alpha\beta}=\left(\frac{n}{m}\right)^2[D_{\alpha\beta}(m)+D_{\alpha\beta}(-m)-2D_{\alpha\beta}(0)],\ \alpha\neq\beta$$

where

$$D_{11}(m)=-\frac{(n+m)x}{nr^2},\ D_{22}(m)=-\frac{(n-m)x}{nr^2}, \tag{C22}$$

$$D_{12}(m)=-D_{21}(m)=-\frac{2(n+m)h}{nr^2},\ r^2=x^2+(n+m)^2h^2$$

for $\rho>1$, and

$$D_{11}(m)=\frac{x}{r^2},\ D_{22}(m)=\frac{x-4mh}{r^2} \tag{C23}$$

$$D_{12}(m)=-D_{21}(m)=\frac{2h}{r^2},\ r^2=(x+2mh)^2+(2nh)^2$$

for $-1<\rho<1$.

ANNOUNCEMENT AND CALL FOR PAPERS

For a Symposium on

INTERFACIAL PHENOMENA in VISCOELASTIC FLOWS

1991 ASME Applied Mechanics/Bioengineering Meeting

The Ohio State University
Columbus, Ohio
June 16–19, 1991

The Fluid Mechanics Committee of the Applied Mechanics Division of the ASME is sponsoring a Symposium on interfacial phenomena in viscoelastic flows. The interfaces can be fluid/gas, fluid/fluid, or fluid/solid. Phenomena considered could include (but are not restricted to) extrudate swell, adhesion phenomena, and free surface instabilities associated with such flows as fiber spinning, mold filling, extrudate swell, and related transitional flows and coating flows.

Extended abstracts should be submitted to the session organizer listed below by Oct. 1, 1990, in three copies. These abstracts will be reviewed and authors notified of acceptance or rejection by Nov. 15, 1990.

Inquiries concerning this Symposium should be addressed to the organizer:

Stephen Bechtel
Department of Engineering Mechanics
The Ohio State University
155 West Woodruff Avenue
Columbus, Ohio 43210
(614) 292-6570
FAX (614) 292-9021